Extremes of the pinch-off location and time in a liquid column by an accelerating solid sphere

Seong Jin Kim,[1,2] Seungho Kim,[1] and Sunghwan Jung[1,*]
[1]*Department of Biomedical Engineering and Mechanics, Virginia Tech, Blacksburg, Virginia 24061, USA*
[2]*Computational Science Research Center, Korea Institute of Science and Technology, Seoul 02792, Korea*

(Received 10 November 2017; published 21 August 2018)

When a solid body rises from a bath, a liquid column is formed and stretched until pinch-off occurs at different locations and times. In the present paper, we study the temporal and spatial evolution of a less viscous liquid column extracted by an accelerating sphere from a bath. At high acceleration, the observed liquid column has the shape of an up-pointing cone, which implies that the column near the sphere is stretched so quickly that the liquid cannot keep up with it. This causes the liquid column to pinch off at the upper location. At low accelerations, a liquid column pinches off at a lower location near the free surface. The shift in the pinch-off location is explained by the axial velocity-gradient profile in the liquid column. The numerical results show that the gradient of the axial velocity near the sphere increases when the solid sphere has a higher acceleration. As a result, at high accelerations, the axial velocity gradient is responsible for the necking and pinching off at the upper location of the liquid column. At low sphere accelerations, the column pinches off at the lower location by the strong Laplace pressure due to the higher gradient of the interfacial curvature between the column and the bath. Next the pinch-off time is observed to decrease as the acceleration increases regardless of the pinch-off location. We use a linear stability analysis to predict the pinch-off time as the inverse of the growth rate in the dispersion relation.

DOI: 10.1103/PhysRevFluids.3.084001

I. INTRODUCTION

The pinch-off dynamics of a liquid column has been extensively studied because of the interesting underlying mechanics [1–3] and its relevance to many engineering applications [4–7]. Plateau first observed that a flowing water column, e.g., water running from a tap, became unstable and that the most unstable wavelength was nearly three times the initial column diameter [8]. Later, Lord Rayleigh showed that the fastest growing wavelength could be predicted using a dispersion relation [9] in which the capillary-inertial wave was considered. Therefore, the pinch-off time t_p is observed to be near the capillary-inertial timescale $\tau_c = \sqrt{\rho_l L^3/\sigma}$, where ρ_l is the liquid density, L is the characteristic length scale (generally the initial diameter of a liquid column), and σ is the surface tension. The pinch-off time is known to be approximately τ_c, unless the diameter of a water column is more than the so-called capillary length [10] $l_c \equiv \sqrt{\sigma/\rho_l g}$, where g is the gravitational acceleration. When $L > l_c$, it pinches off earlier than τ_c because gravity ($\sim\rho_l g$) overwhelms the capillarity ($\sim\sigma$). Similarly, when a liquid column is significantly accelerated by a solid object, the pinch-off time depends on the acceleration timescale τ_a ($=\sqrt{L/a}$) [11–13]. This timescale was derived by considering the extracted liquid mass $\sim\sigma L/a$ by capillary adhesion; then this water mass was used to replace the inertia scale $\sim\rho_l L^3$ in τ_c [11].

*sunnyjsh@vt.edu

In addition to the pinch-off time, the spatial evolution of a liquid column has drawn much attention because of its applications in transferring a liquid volume to a solid surface, which is called the liquid-bridge extension [4–6]. When the capillarity is the only cause for the pinch-off with small gravity and inertia effects, the liquid bridge extends symmetrically and then pinches off in the middle [14]. When a liquid column is held between two solid surfaces with different wettabilities, the liquid column near the more wettable surface becomes thinner faster than the other side does because the larger gradient of the interfacial curvature on the wettable side creates more capillary pumping [15]. When the gravity becomes dominant over the capillarity, the pinch-off location is moved slightly farther from its middle location because most of the liquid is drained by gravity, but the location remains near the middle point [16]. Additionally, a faster extensional speed of the bridge or high viscosity of the liquid is known to delay the pinch-off behavior with the formation of a longer liquid thread [16,17]. When only one end of the solid surface moves quickly, a liquid column pinches off near the fast-moving surface [16].

A solid body that moves from water into air, hereafter referred to as a water-exit body, also exhibits pinch-off behaviors and plays an important role in natural systems [12,18,19] and industrial applications [4,6]. Interestingly, when dogs and cats drink water, they can control the acceleration of their tongues to be in the range of $1g$–$4g$ [12] and $1g$–$2g$ [19], respectively. The pinch-off dynamics of a water column is more affected by gravity when a cat drinks than when a dog drinks [12,19]. From an industrial perspective, understanding the pinch-off dynamics can give engineers better control over the amount of remnant liquid that adheres to a solid body that is withdrawn from a liquid [11], e.g., the dip-coating process [4].

Despite previous studies, the pinch-off location and shape of the water column remain unclear when a solid body exits water. In the present paper, we study a liquid column extended by a solid sphere that rises with constant acceleration from a liquid bath. The pinch-off location depends significantly on the acceleration of the solid sphere when the axial velocity distribution changes in the liquid column. Numerical data show that the acceleration of the solid sphere increases the maximum velocity gradient near the sphere, which contracts the liquid column because of continuity. Moreover, the maximum velocity gradient is observed to decrease over time, which further yields a scaling relation for the pinch-off timescale.

II. METHODS

A. Experiment

The experiment uses a linear stage (BiSlide MB10-0150/Velmex, Inc.) to withdraw a solid sphere from a liquid bath, as illustrated in the inset of Fig. 1(a). A high-speed camera (SC2+/Edgertronic) simultaneously records the images with a frame rate of up to 4000 frames per second. In the experiments, we used two liquids: $[\rho_l\ (\mathrm{kg/m^3}), \sigma\ (\mathrm{mN/m})] = [998, 73]$ for water and $[762, 22]$ for ethanol. The surface tension values of water and ethanol were measured using a surface tensiometer (K11, KRÜSS) based on the Wilhelmy plate method [20]. The diameter of the glass spheres varied from 2.4 to 15.9 mm. The initial position of the sphere was at the free surface of the liquid, and a constant acceleration in the range of 2.1×10^{-2} to $1.5 \times 10^{2}\ \mathrm{m/s^2}$ was applied to the sphere. The pinch-off location z_p and the center position of the sphere Z_p at the pinch-off moment were measured from the free surface. The vertical coordinates of z and Z were positive above the free surface and negative otherwise.

B. Numerical simulation

To better understand how the acceleration of a sphere affects the pinch-off dynamics, the liquid flow for different accelerations was numerically calculated. We performed this numerical simulation using the open-source code called GERRIS [21,22], which has been widely used in the academic community to effectively simulate interfacial behaviors [23]. In the simulation, the temporal evolution of the axial velocity distribution in a liquid column was investigated with different sphere accelerations in the

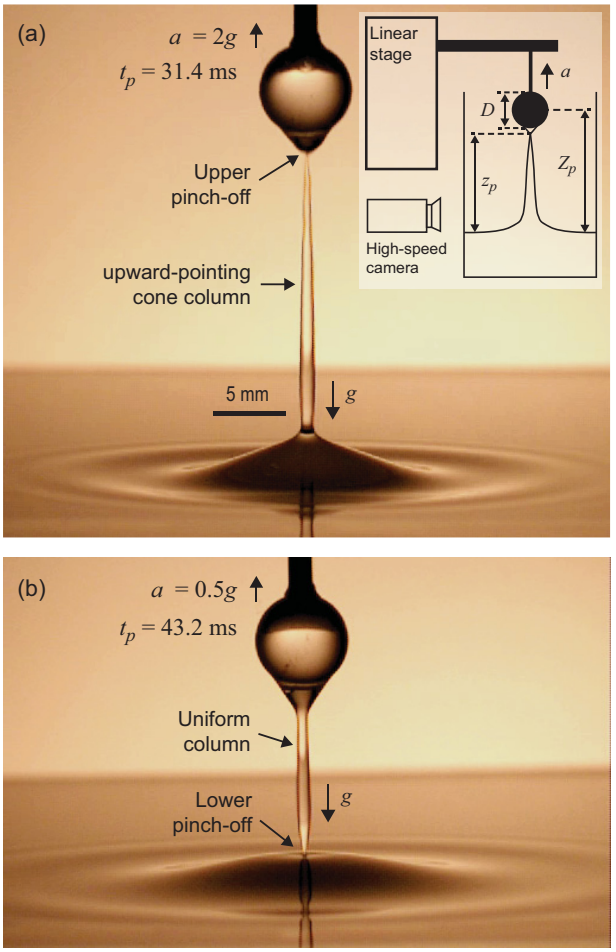

FIG. 1. Shapes of a water column: (a) an upward-pointing cone column with upper pinch-off and (b) a uniform column diameter in the middle with lower pinch-off. Here a glass sphere of $D = 6.35$ mm was withdrawn from a water bath with constant acceleration of (a) $a = 2g$ or (b) $0.5g$. The pinch-off time was measured to be (a) 31.4 ms and (b) 43.2 ms. The inset in (a) illustrates the experimental schematic of ascending a solid sphere with a constant acceleration that is controlled by the linear stage. Here z_p is the pinch-off location and Z_p is the center position of the sphere from the free surface at the pinch-off moment.

moving frame that followed the center of the sphere. In GERRIS, the continuity and Navier-Stokes equations for incompressible fluids are solved axisymmetrically in cylindrical coordinates using the volume of fluid method to track the liquid-air interface [21,24]:

$$\nabla \cdot \mathbf{u} = 0, \tag{1a}$$

$$\rho \frac{D\mathbf{u}}{Dt} = -\nabla p + \nabla \cdot [\mu(\nabla \mathbf{u} + \nabla \mathbf{u}^T)] + \sigma \kappa \mathbf{n} \delta_s(c) + \rho \mathbf{g} - \rho \mathbf{a}, \tag{1b}$$

$$\frac{\partial c}{\partial t} + \nabla \cdot (c\mathbf{u}) = 0, \tag{1c}$$

$$\rho = c\rho_l + (1 - c)\rho_a, \tag{1d}$$

$$\mu = c\mu_l + (1 - c)\mu_a, \tag{1e}$$

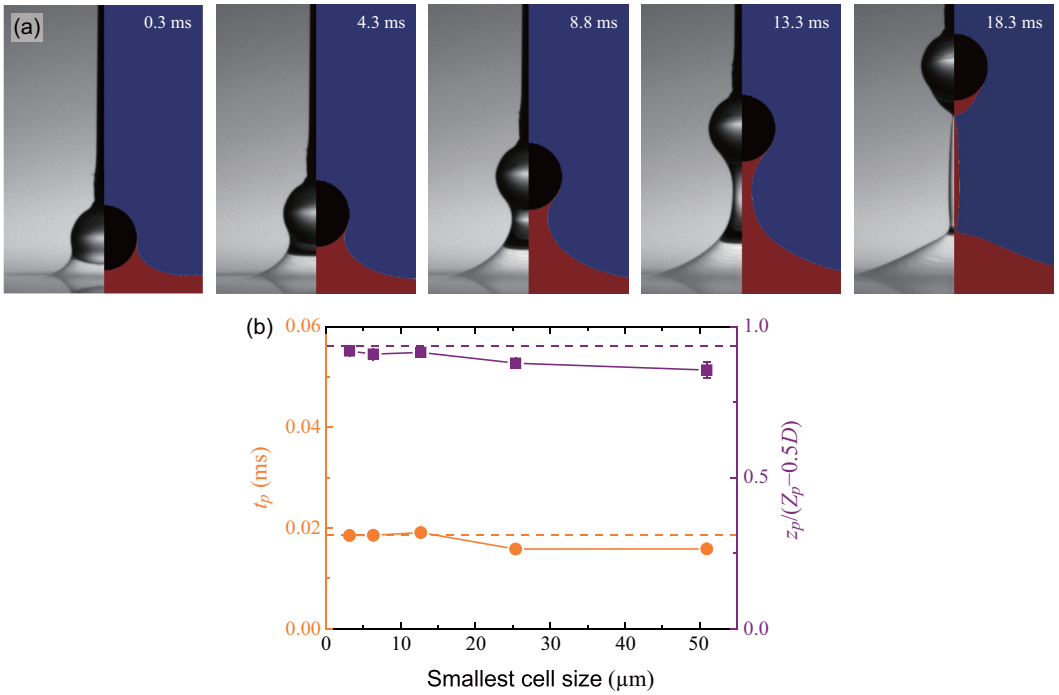

FIG. 2. (a) Temporal evolution of the water-air interface when a glass sphere of $D = 3.2$ mm rises at $a = 2g$. Experimental images and numerical results from GERRIS are compared side-to-side at different times: $t = 0.3$, 4.3, 8.8, 13.3, and 18.3 ms. (b) Comparison of pinch-off time t_p and normalized pinch-off location $z_p/(Z_p - 0.5D)$ between the experiment and simulation results with a changing minimal mesh size. In the present study, the simulation results are obtained only with smallest mesh size $\leqslant 6.3$ μm after the data converge.

where $\mathbf{u}$ is the fluid velocity vector, p is the pressure, κ is the interface curvature, $\mathbf{n}$ is the unit normal vector to the interface, and $\mathbf{g}$ is the gravitational acceleration vector. Here c is the fraction function that is a scalar function of spatial and temporal coordinates [24]. The c is defined to be unity in the liquid and zero in air; otherwise $0 < c < 1$ at the liquid-air interface. Then the fluid density and viscosity of different phases are determined by Eqs. (1d) and (1e): ρ_l (=998 kg/m^3 for water and 762 kg/m^3 for ethanol) and ρ_a (=1.2 kg/m^3) are the liquid and air densities, respectively, and μ_l (=1.0×10^{-3} kg/m s for water and 1.1×10^{-3} kg/m s for ethanol) and μ_a (=1.9×10^{-5} kg/m s) are the liquid and air viscosities, respectively. The value of the function $\delta_s(c)$ is unity at the interface ($0 < c < 1$) and zero elsewhere, so the surface tension force acts only at the liquid-air interface. For the Navier-Stokes equation (1b), we consider the noninertial frame by adding the translational inertia $\rho\mathbf{a}$ [25,26]. In the moving frame, the origin of the cylindrical coordinates is at the center of the solid sphere. Initially, the liquid-air interface is flat on the same vertical line as the center of the sphere. Then both air and liquid begin to flow down by setting the fluid velocity that accelerates with a at the top and bottom boundaries. The detailed code used for running numerical simulations is available in the Supplemental Material [27]. The numerical data calculated in the moving frame are postprocessed using an in-house *Mathematica* code to obtain $\mathbf{u}(t, z)$ and the interfacial coordinates in the stationary frame with the vertical origin at the free surface. For the contact line motion, we nominally impose the no-slip boundary condition on the solid sphere. Nevertheless, the present computation scheme using the volume of fluid method in GERRIS is considered to have an implicit slip length, even for the no-slip boundary condition [28,29]. This occurs because the liquid-air interface is calculated as

being advected by Eq. (1c) with a velocity calculated in a mesh and not on an edge on the solid surface. Therefore, it has the implicit or effective slip length of approximately half the mesh size.

The temporal evolution of the interfacial shape is compared between experiments and simulations as shown in Fig. 2(a), which shows consistency. For both experiment and simulation, a sphere of $D = 3.2$ mm rises from water with $a = 2g$. In the study, t is set to zero when the bottom of the solid sphere reaches the free surface, so it begins to exit the liquid. The numerical convergence is checked by looking at the pinch-off time t_p and normalized pinch-off location $z_p/(Z_p - 0.5D)$ versus the smallest mesh size, as shown in Fig. 2(b). The simulation results approach the experimental values (dashed lines) as the mesh size decreases and converge at the level below the smallest mesh size of 12.7 μm. In this present paper, the simulation results with the smallest mesh size of 6.3 μm (=0.5 × 12.7 μm) after the convergence are used as the simulation data. Here the pinch-off location is normalized by the distance between the free surface and the bottom of the sphere, so a value near unity indicates an upper pinch-off. Otherwise, a normalized pinch-off location that approaches zero indicates a lower pinch-off.

III. RESULT AND DISCUSSION

A. Column evolution with different sphere accelerations

Figures 1(a) and 1(b) show two representative cases of a sphere ($D = 6.35$ mm) being accelerated at $a = 2g$ and $0.5g$, respectively. The pinch-off location dramatically shifts from upper [Fig. 1(a)] to lower [Fig. 1(b)] locations. The column shape is near an upward-pointing cone at a high acceleration [Fig. 1(a)] but has a uniform diameter in the middle at a low acceleration [Fig. 1(b)]. The upward-pointing cone shape implies that the water column is stretched, but the water cannot keep up with the solid sphere. Therefore, the column likely pinches off near the sphere. A similar up-triangular column was also experimentally [12,19] and numerically [16] observed in previous literature.

In contrast, a uniform column is observed when a sphere rises at a low acceleration or almost constant speeds [10]. The fast-moving sphere stretches the liquid column into a thin ligament with a small variation in curvature [10]. In this case, a lower pinch-off location is more likely to occur because of a high curvature gradient, which creates stronger capillary pumping back to the bath. From this point, the lower location is the most probable place to pinch off because a higher curvature gradient is consistently observed near the free surface in the present experiments. In addition to the capillary pumping at the bottom, one may discuss the gravitational drainage for the case of a low acceleration. A previous study on the liquid bridge stretched by circular solid disks with the same diameter [16] showed that the liquid bridge pinches off near the middle of the bridge when it is governed by capillarity. However, when the gravity is dominant over the capillarity, the pinch-off location moves up slightly but remains near the middle point because some liquid inside the bridge is drained down by gravity [16]. In the present liquid-exit experiment, this behavior is not observed, presumably due to the stronger capillary pumping at the bottom with a higher curvature gradient near the free surface.

Figure 3(a) shows the *normalized* pinch-off location versus the acceleration-based Bond number $\mathrm{Bo}_a = \rho_l a D^2/\sigma$ [11]. The pinch-off near the middle location (slightly below the middle location) occurs only when a liquid column extends quasistatically as $\mathrm{Bo}_a \to 0$ [18]. As Bo_a increases, the pinch-off location moves relatively to a lower location in the liquid column [$z_p/(Z_p - 0.5D) \to 0$]. As previously mentioned, when acceleration a is lower than g (or $a/g < 1$), the liquid column more likely pinches off near the free surface. Figure 3(b) presents the *absolute* pinch-off location from the free surface, which shows that the liquid column pinches off near the free surface ($\approx 0.2D$) for Bo_a up to the transition regime ($\mathrm{Bo}_a \leqslant 1$). However, the pinch-off location relative to the column height decreases because the column height at the pinch-off moment Z_p increases with Bo_a. When $\mathrm{Bo}_a \gg 1$ or the acceleration is sufficiently high such that $a \gg g$, pinch-off occurs in the upper location as shown in Fig. 3(a). The pinch-off location gradually decreases to approximately zero as Bo_a increases when $a/g < 1$. Similarly, for the upper pinch-off cases, the normalized pinch-off location increases

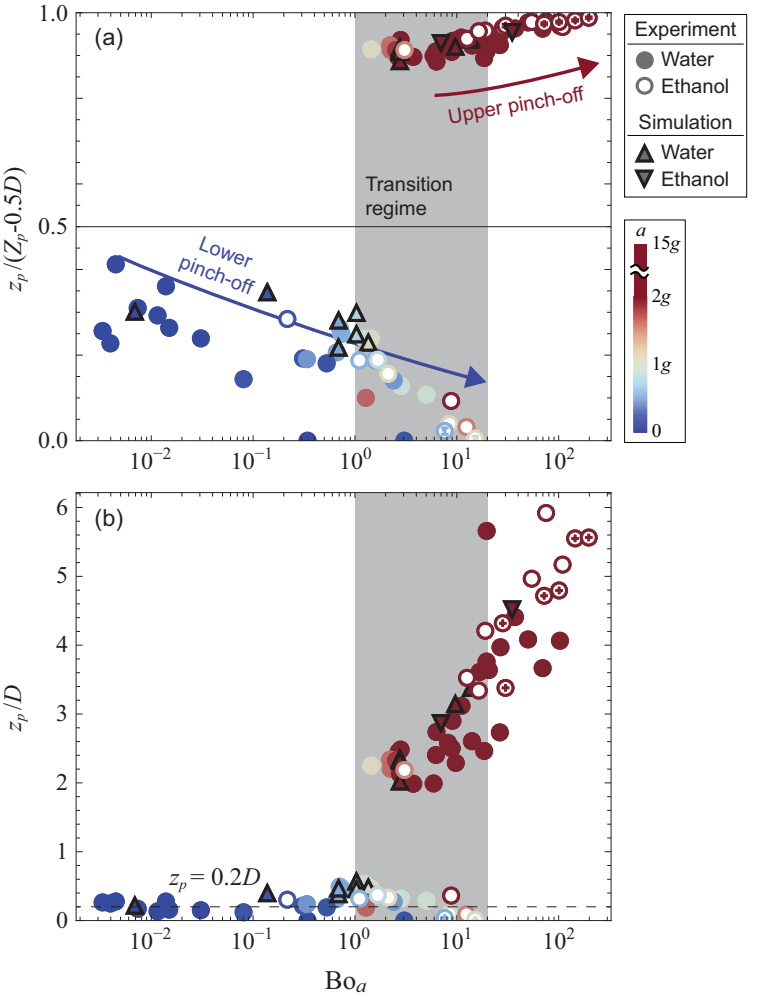

FIG. 3. Shift in the pinch-off location by the acceleration-based Bond number $\mathrm{Bo}_a = \rho_l a D^2/\sigma$. The pinch-off location is presented by (a) the relative location in the liquid column, which is estimated by the normalized pinch-off location $z_p/(Z_p - 0.5D)$, and (b) the absolute location from the free surface, which is estimated by z_p/D. The data are colored according to the acceleration of the solid sphere. Circles and triangles indicate experimental and simulation data, respectively.

to unity (near the sphere) as Bo_a increases. The gray highlighted region ($1 \lesssim \mathrm{Bo}_a \lesssim 20$) indicates a transition regime, where both lower and upper pinch-offs coexist and occur almost simultaneously or within a short time interval of less than 1 ms. This concurrent pinch-off can be rationalized by the fact that the effects of both capillary pumping and column stretching are of the same order of magnitude, as discussed in the previous literature [11].

B. Temporal evolution of the axial velocity in the liquid column

Figure 4 presents the numerical results of the temporal evolution of the axial velocity $\tilde{u}_z(\tilde{t}, \tilde{z})$ for two different accelerations $0.5g$ and $2g$, where the numerical data are plotted in dimensionless form. The length and timescales are nondimensionalized using the sphere diameter of D and capillary-inertial timescale of τ_c ($=\sqrt{\rho_l D^3/\sigma}$), respectively; then the tilde indicates a dimensionless quantity.

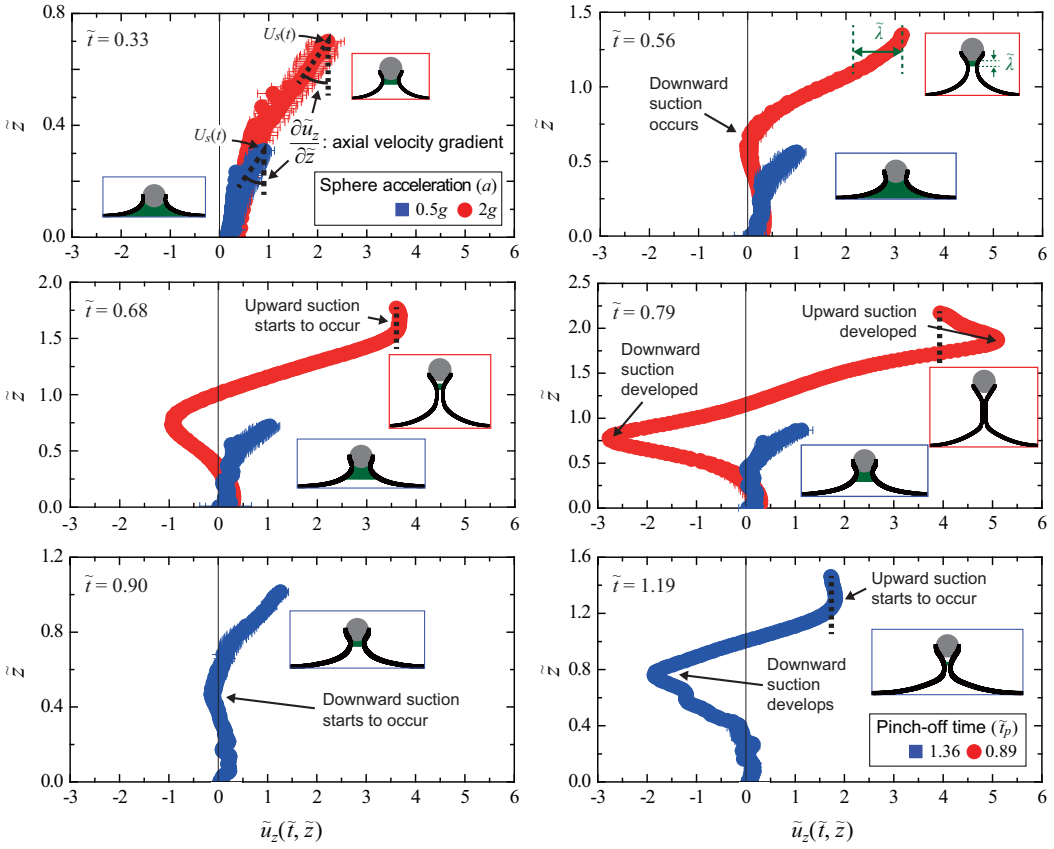

FIG. 4. Temporal and spatial evolution of the axial velocity, which is radially averaged in a water column formed by a rising solid sphere with different accelerations of $0.5g$ (blue) and $2g$ (red). The axial velocity at the highest $\tilde{z}$ equals the instantaneous velocity of an accelerating sphere $U_s(t)$, as shown in the subplot at $\tilde{t} = 0.33$. The axial velocity is numerically calculated using the open-source code named GERRIS [21]. For simulations, the initial and boundary conditions are maintained with $D = 3.2$ mm, $\rho_l = 998\,\mathrm{kg/m^3}$, and $\sigma = 0.073$ N/m, except for the acceleration of the sphere. The shapes of the water-air interface are presented in the insets with blue and red borders for $a = 0.5g$ and $2g$, respectively. The dark green regions indicate the decaying length defined in Sec. III C.

Then $\tilde{u}_z$ is nondimensionalized by D and τ_c as $\tilde{u}_z = u_z/u_c$, where $u_c = \sqrt{\sigma/\rho_l D}$ is the capillary-inertial velocity [30]. The axial velocity is radially averaged in a liquid column, and the horizontal error bars indicate the standard deviations at each vertical location $\tilde{z}$. The radial velocity $\tilde{u}_r$ is observed to be negligible compared to $\tilde{u}_z$, except very early in time. For each time step $\tilde{t}$, the averaged axial velocity is presented in the range of $0 \leqslant \tilde{z} \leqslant \tilde{Z}(\tilde{t}) - 0.5$, where $\tilde{Z}(\tilde{t}) - 0.5$ is at the bottom of a sphere. In all simulations in Fig. 4, the solid and fluid conditions are the same ($D = 3.2$ mm, $\rho_l = 998\,\mathrm{kg/m^3}$, and $\sigma = 0.073\,\mathrm{N/m}$). An interesting observation is that the velocity gradient $\partial\tilde{u}/\partial\tilde{z}$ near the sphere increases with the acceleration. Such a high gradient in the axial velocity escalates the column-necking behavior near the sphere because the radial velocity is proportional to the gradient in the axial velocity according to the fluid continuity, $\partial\tilde{r}(\tilde{t}, \tilde{z})/\partial\tilde{t} = -0.5\tilde{r}\partial\tilde{u}_z(\tilde{t}, \tilde{z})/\partial\tilde{z} - \tilde{u}_z\partial\tilde{r}/\partial\tilde{z}$, where $\tilde{r}(\tilde{t}, \tilde{z})$ is the column radius. Then the narrowing column pumps the water towards the sphere due to the pressure gradient induced by a high curvature gradient.

For the higher acceleration case of $a = 2g$, the upward suction becomes even faster than the velocity of the sphere as $\tilde{t}$ surpasses 0.68, which causes the upper pinch-off at higher accelerations.

This suction speed increases significantly as the column becomes narrower over time. However, at $\tilde{t} = 0.56$, which is earlier than the time when the upward suction emerges, a downward suction begins to develop near the free surface. This downward suction further increases with $\tilde{t}$ (as shown at $\tilde{t} = 0.68$ and 0.79 in Fig. 4). Although the downward suction occurs before the upward suction, it is difficult to pinch off a thicker liquid column near the free surface earlier than a thinner column neck near the sphere. Moreover, near the free surface, the liquid is continuously supplied from the upper part of the column as the liquid flows down. In contrast, the liquid column near the sphere cannot be supplied from a lower part because the upper sphere continues accelerating. Eventually, the liquid column is pinched off at the upper location first.

For the case of low acceleration (e.g., $a = 0.5g$), downward suction near the bath starts earlier and proceeds faster than column necking near the sphere. The upward suction near the sphere begins at approximately $\tilde{t} = 1.19$, but it is rather late to overcome the column necking that has already developed. The velocity of the downward suction reaches $\tilde{u}_z \approx -2$. It is contrasted with the case of $a = 2g$, where the downward suction remains approximately $\tilde{u}_z \approx -1$ at $\tilde{t} = 0.68$ when the upward suction begins to occur. Likewise, at low acceleration, the upward suction is not so effective that the liquid column pinches off at the upper location; instead, it pinches off at the lower location, where the downward suction velocity increases significantly ($\tilde{t}_p = 1.36$). It should be noted that the wavy pattern of the axial velocity along the liquid column near the free surface for $a = 0.5g$ is due to the capillary force, which is similar to the capillary wave of the liquid jet impinging on a liquid reservoir [31].

In Fig. 4, the data for $a = 2g$ are not presented from $\tilde{t} = 0.90$ because they pinched off at the early time of $\tilde{t}_p = 0.89$ by the upward suction near the sphere. Here we conclude that the high velocity gradient induced by the high acceleration of a sphere causes the upper pinch-off when it yields the upward suction near the sphere sufficiently to overcome the downward velocity near the bath.

C. Evolution of the maximum velocity gradient

Figure 5(a) presents the temporal evolution of the maximum velocity gradient $\partial\tilde{u}_z/\partial\tilde{z}$ near the sphere for high accelerations of $2g$, $7g$, and $10g$ on the left and low accelerations of $0.5g$, $0.75g$, and $1g$ on the right. The maximum velocity gradient is calculated as the maximum gradient of an axial velocity along the column; then it is nondimensionalized by multiplying τ_c. We find that the maximum velocity gradient decreases over time following the slope of $-1/2$ in the log-log scale. The maximum velocity gradient diverges near the pinch-off moment due to the upward suction. As shown in Sec. III B, this divergence emerges sooner with a higher sphere acceleration. A previous study [32] showed that such a log-log dependence with an exponent of 1/2 was also observed for the capillary-inertial decay length $\tilde{\lambda}$, where the axial velocity evolved as $\sim\tilde{t}^{1/2}$ for an impulsively stretching water column [32]. In addition, a self-similar variable such as $\tilde{u} = U(\tilde{z}/\tilde{t}^{1/2})$ is known to govern the universal pinch-off dynamics very close to the pinch-off moment [3]. A similar observation on the self-similarity was also discussed for the planar rupture of thin liquid films [33].

To discuss this result of the decay length in the present study, the $\tilde{\lambda}$ is estimated to be the distance from the z location of reaching the maximum velocity of $\tilde{u}_z$ to the lower z location, where $\tilde{u}_z$ decays by 1. This decay length from the simulations is illustrated as a dark green region in the liquid column in the insets of Fig. 4. Figure 5(b) shows the temporal evolution of $\tilde{\lambda}$ for high acceleration on the left and low acceleration on the right. We observe that $\tilde{\lambda}$ evolves as $\tilde{\lambda} = (1/4.5)\tilde{t}^{1/2}$, as found in the above self-similar result. We also remark that our measured $\tilde{\lambda}$ is approximately the inverse of the maximum $\partial\tilde{u}_z/\partial\tilde{z}$. This trend becomes clearer as the sphere acceleration increases from $0.5g$ to $10g$ presumably because the one-dimensional approximation holds well for a slender liquid column generated by a sphere with high acceleration. Although the values of $\tilde{\lambda}$ are similar for different accelerations, the ratio of $\tilde{\lambda}$ to the water column height $\tilde{Z}$ varies significantly, as shown in the insets of Fig. 4. For low acceleration in the insets with the blue edge, $\tilde{\lambda}$ covers the entirety or most of the water column, which indicates that the axial velocity decreases slowly along almost the entire column. However, for high accelerations, $\tilde{\lambda}$ fills in only a small portion of the upper part in a water

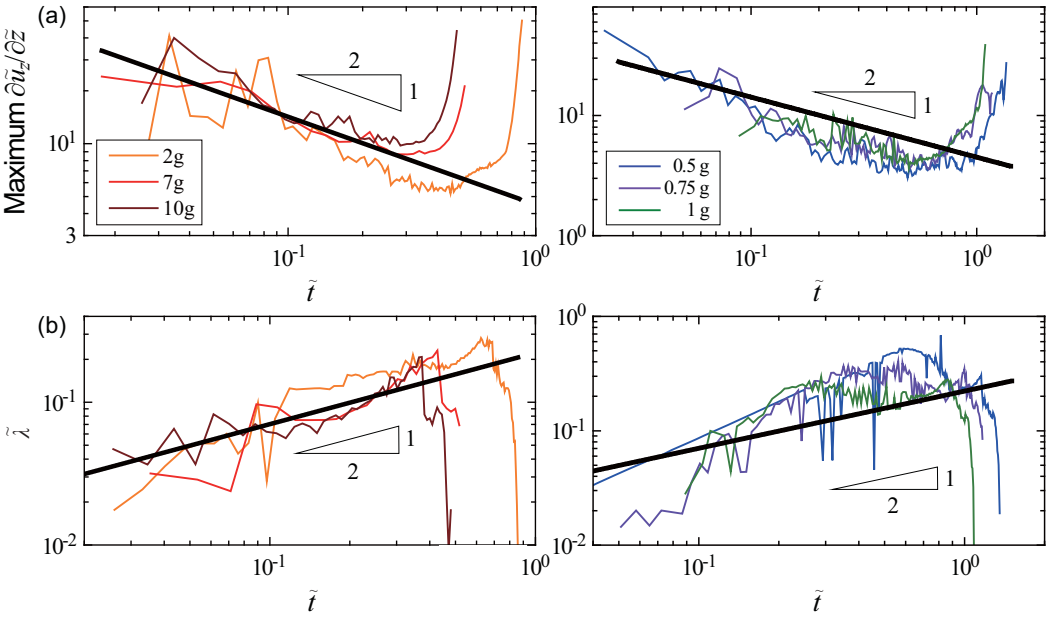

FIG. 5. Numerical data on the temporal evolution of the (a) dimensionless maximum velocity gradient and (b) decaying length for high accelerations of $2g$, $7g$, and $10g$ on the left and low accelerations of $0.5g$, $0.75g$, and $1g$ on the right. The black lines indicate (a) $(\partial\tilde{u}_z/\partial\tilde{z})_{\max} = 4.5\tilde{t}^{-1/2}$ and (b) $\tilde{\lambda} = (1/4.5)\tilde{t}^{1/2}$.

column, as presented in the insets with the red edge; therefore, only the nearby water can follow the moving sphere in contrast to the case of low acceleration. Accordingly, a water volume in the upper part of the column decreases faster for higher acceleration, which causes the column necking and further upward suction, as discussed in Sec. III B. Thus, it is anticipated that the upper pinch-off occurs when the decay length is much smaller than the column height, $\tilde{\lambda} \ll \tilde{Z}$. Using the predicted pinch-off time that will be derived in the next section ($\tilde{t}_p = \sqrt{8\pi/9}\mathrm{Bo}_a^{-1/2}$), the decay length at the moment of pinch-off is $\tilde{\lambda} = (1/3)(8\pi/9)^{1/4}\mathrm{Bo}_a^{-1/4}$. For cases of high acceleration ($\mathrm{Bo}_a > 1$), the maximum decay length is $(1/3)(8\pi/9)^{1/4} \simeq 0.43$, which implies that no more than one-half of the diameter is a characteristic distance, where a liquid column is affected by the acceleration and follows the moving solid. At pinch-off, the column height is always taller than the decay length. Therefore, we anticipate that the pinch-off occurs near the moving sphere.

D. Pinch-off time

In this section, we predict the pinch-off time using a linear analysis, which characterizes both the temporal and spatial changes in the velocity and radius of a liquid column. To simplify the analysis, we assume that the column is axisymmetric over time and that the viscous effect is negligible. Then the one-dimensional governing equations of a liquid column can be written in dimensional form as [34]

$$\rho_l\left(\frac{\partial u_z}{\partial t} + u_z\frac{\partial u_z}{\partial z}\right) = -\frac{\partial p}{\partial z} - \rho_l g, \tag{2a}$$

$$\frac{\partial r}{\partial t} = -u_z\frac{\partial r}{\partial z} - \frac{r}{2}\frac{\partial u_z}{\partial z}, \tag{2b}$$

where the capillary pressure is approximated as $p \simeq \sigma[1/r - \partial^2 r/\partial z^2]$ and $r(z,t)$ is the radius of a liquid column. We assume two normal modes: one for the axial velocity $[u_z(z,t) = u_{z0}(1 -$

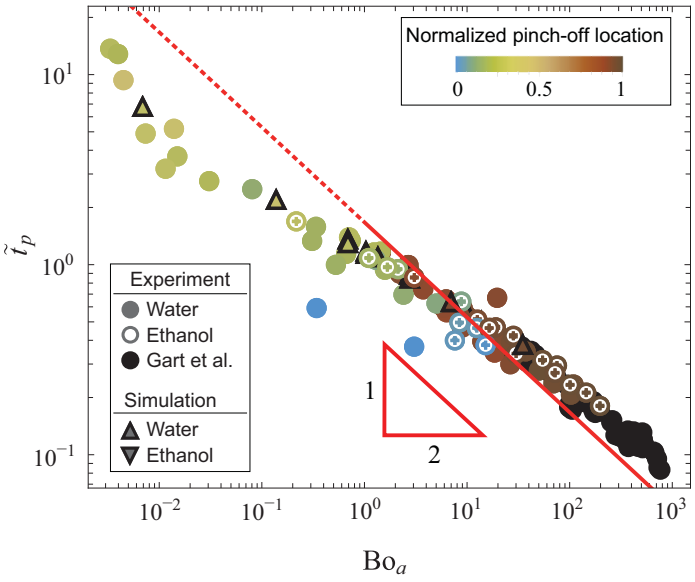

FIG. 6. Dimensionless pinch-off time $\tilde{t}_p$ versus acceleration-based Bond number ($=\rho_l a D^2/\sigma$). The red line indicates the present theory of $\tilde{t}_p = \sqrt{8\pi/9}\mathrm{Bo}_a^{-1/2}$ for the high acceleration of a sphere.

$\epsilon e^{\omega t+ikz}$)] and the other for the radius of the column [$r(z,t) = r_0(1-\epsilon e^{\omega t+ikz})$]. Here the first-order perturbation is at frequency ω and wave number k, r_0 is the initial radius of the liquid column, and $u_{z0} = at$ is the velocity of the sphere. Then the above equations on the order of ϵ become $a + \omega(at) + ik(at)^2 = (\sigma/\rho)r_0 ik(1/r_0^2 - k^2)$ and $\omega = -(3/2)\,ik\,(at)$. Finally, we obtain a dispersion relation

$$\omega^2 = \frac{9}{2}\left[\frac{\sigma}{\rho_l r_0^3}(kr_0)^2[1-(kr_0)^2] + iak\right]. \tag{3}$$

This dispersion relation describes how the temporal frequency (inverse of the timescale) is related to the spatial wave number (inverse of the length scale). Thus, we anticipate that the real part of the frequency ω_r should be related to the inverse of the pinch-off time as $\omega_r \simeq 2\pi/t_p$. On the right-hand side of Eq. (3), two main terms appear: The first term depends on the capillarity and the second one depends on the acceleration.

For cases of high acceleration ($\mathrm{Bo}_a > 1$), the unsteady inertia from the acceleration of a sphere is dominant. Experimentally, we observe that the pinch-off occurs right below a sphere, which suggests that the pinch-off wave number of interest is $k \simeq 2\pi/D$. Then the predicted pinch-off time becomes $t_p = 2\pi[(9\pi/2)(a/D)]^{-1/2} = (2/3)\sqrt{2\pi}\,\sqrt{D/a}$. In nondimensional form, $\tilde{t}_p = \sqrt{8\pi/9}\mathrm{Bo}_a^{-1/2}$. As shown in Fig. 6, the nondimensionalized pinch-off times are found to collapse along the predicted pinch-off time from the linear stability (a red line) when $\mathrm{Bo}_a > 1$. The circles and triangles indicate the experimental and numerical data, respectively. There is also consistency with the previous data from similar experiments of pulling a glass rod out of water as presented by black circles in Fig. 6 [12].

IV. CONCLUSION

The pinch-off locations and time were studied for a liquid column stretched by a solid sphere, which rises with constant acceleration. We have found that the pinch-off location is substantially affected by the acceleration of the sphere. Different accelerations change the profile of the axial velocity in the liquid column. A high velocity gradient near the sphere creates the upper pinch-off by

vertically stretching the nearby liquid column and consequently forming an upward-pointing cone. This velocity gradient is estimated as the capillary-inertial decaying length near the sphere based on the numerical results, which is consistent with the previous literature. In the opposite case of low acceleration, it pinches off at the lower location due to the downward capillary suction, which is induced by a Laplace pressure gradient between a high-pressure column and a low-pressure bath. Moreover, a linear stability analysis predicts the pinch-off time to be $\tilde{t}_p = \sqrt{8\pi/9}\mathrm{Bo}_a^{-1/2}$ for high acceleration, which describes our experimental results quite well.

ACKNOWLEDGMENTS

This work was partially supported by the National Science Foundation (Grant No. CBET-1604424). S.J.K. also acknowledges support from the Disaster and Safety Management Institute funded by Korea Coast Guard through Grant No. KCG-01-2017-02.

[1] J. Eggers and E. Villermaux, Physics of liquid jets, Rep. Prog. Phys. **71**, 036601 (2008).
[2] J. Eggers, Theory of drop formation, Phys. Fluids **7**, 941 (1995).
[3] J. Eggers, Universal Pinching of 3D Axisymmetric Free-Surface Flow, Phys. Rev. Lett. **71**, 3458 (1993).
[4] B. Shang, X. Yu, H. Zheng, B. Xie, Q. Chen, and X. Luo, Numerical and experimental study on the transferred volume in phosphor dip-transfer coating process of light-emitting diodes packaging, J. Electron. Packag. **138**, 021003 (2016).
[5] C. Xu, Z. Zhang, J. Fu, and Y. Huang, Study of pinch-off locations during drop-on-demand inkjet printing of viscoelastic alginate solutions, Langmuir **33**, 5037 (2017).
[6] S. Kumar, Liquid transfer in printing processes: Liquid bridges with moving contact lines, Annu. Rev. Fluid Mech. **47**, 67 (2015).
[7] I. Frankel and D. Weihs, Stability of a capillary jet with linearly increasing axial velocity (with application to shaped charges), J. Fluid Mech. **155**, 289 (1985).
[8] J. A. F. Plateau, *Statique Expérimentale et Théorique des Liquides Soumis aux Seules Forces Moléculaires* (Gauthier-Villars, Paris, 1873), Vol. 2.
[9] Lord Rayleigh, On the instability of jets, Proc. Lond. Math. Soc. **1**, 4 (1878).
[10] P. Marmottant and E. Villermaux, Fragmentation of stretched liquid ligaments, Phys. Fluids **16**, 2732 (2004).
[11] L. Vincent, L. Duchemin, and E. Villermaux, Remnants from fast liquid withdrawal, Phys. Fluids **26**, 031701 (2014).
[12] S. Gart, J. J. Socha, P. P. Vlachos, and S. Jung, Dogs lap using acceleration-driven open pumping, Proc. Natl. Acad. Sci. USA **112**, 15798 (2015).
[13] C. Weickgenannt, I. V. Roisman, and C. Tropea, Pinch-off of a stretching viscous filament and drop transport, New J. Phys. **17**, 083059 (2015).
[14] Y.-J. Chen and P. Steen, Dynamics of inviscid capillary breakup: Collapse and pinchoff of a film bridge, J. Fluid Mech. **341**, 245 (1997).
[15] S. Dodds, M. Carvalho, and S. Kumar, Stretching liquid bridges with moving contact lines: The role of inertia, Phys. Fluids **23**, 092101 (2011).
[16] X. Zhang, R. Padgett, and O. Basaran, Nonlinear deformation and breakup of stretching liquid bridges, J. Fluid Mech. **329**, 207 (1996).
[17] O. E. Yildirim and O. A. Basaran, Deformation and breakup of stretching bridges of Newtonian and shear-thinning liquids: Comparison of one-and two-dimensional models, Chem. Eng. Sci. **56**, 211 (2001).
[18] S. J. Kim, J. Hasanyan, B. J. Gemmell, S. Lee, and S. Jung, Dynamic criteria of plankton jumping out of water, J. R. Soc. Interface **12**, 20150582 (2015).

[19] P. M. Reis, S. Jung, J. M. Aristoff, and R. Stocker, How cats lap: Water uptake by Felis catus, Science **330**, 1231 (2010).
[20] L. Wilhelmy, Ueber die abhängigkeit der capillaritäts-constanten des alkohols von substanz und gestalt des benetzten festen körpers, Ann. Phys. (Leipzig) **195**, 177 (1863).
[21] S. Popinet, Gerris: A tree-based adaptive solver for the incompressible Euler equations in complex geometries, J. Comput. Phys. **190**, 572 (2003).
[22] S. Popinet, An accurate adaptive solver for surface-tension-driven interfacial flows, J. Comput. Phys. **228**, 5838 (2009).
[23] S. Popinet, Numerical models of surface tension, Annu. Rev. Fluid Mech. **50**, 49 (2018).
[24] C. W. Hirt and B. D. Nichols, Volume of fluid (VOF) method for the dynamics of free boundaries, J. Comput. Phys. **39**, 201 (1981).
[25] I. M. Gledhill, H. Roohani, K. Forsberg, P. Eliasson, B. W. Skews, and J. Nordström, Theoretical treatment of fluid flow for accelerating bodies, Theor. Comput. Fluid Dyn. **30**, 449 (2016).
[26] A. G. Gardi, Moving reference frame and arbitrary Lagrangian Eulerian approaches for the study of moving domains in Typhon, Masters thesis, Politecnico di Milano, 2011.
[27] See Supplemental Material at http://link.aps.org/supplemental/10.1103/PhysRevFluids.3.084001 for the details of the code to run the numerical simulation of GERRIS.
[28] S. Afkhami, S. Zaleski, and M. Bussmann, A mesh-dependent model for applying dynamic contact angles to VOF simulations, J. Comput. Phys. **228**, 5370 (2009).
[29] J. Moriarty and L. Schwartz, Effective slip in numerical calculations of moving-contact-line problems, J. Eng. Math. **26**, 81 (1992).
[30] S. Schiaffino and A. A. Sonin, Molten droplet deposition and solidification at low Weber numbers, Phys. Fluids **9**, 3172 (1997).
[31] M. J. Hancock and J. W. Bush, Fluid pipes, J. Fluid Mech. **466**, 285 (2002).
[32] L. Duchemin, S. Le Dizès, L. Vincent, and E. Villermaux, Self-similar impulsive capillary waves on a ligament, Phys. Fluids **27**, 051704 (2015).
[33] S. S. Thete, C. Anthony, P. Doshi, M. T. Harris, and O. A. Basaran, Self-similarity and scaling transitions during rupture of thin free films of Newtonian fluids, Phys. Fluids **28**, 092101 (2016).
[34] J. Eggers and T. F. Dupont, Drop formation in a one-dimensional approximation of the Navier-Stokes equation, J. Fluid Mech. **262**, 205 (1994).